© 2016. Published by The Company of Biologists Ltd | Journal of Cell Science (2016) 129, 2865-2875 doi:10.1242/jcs.190843

TOOLS AND TECHNIQUES

Multifunctional *in vivo* imaging of pancreatic islets during diabetes development

Ge Li[1], Binlin Wu[1,*], Meliza G. Ward[1], Angie C. N. Chong[2], Sushmita Mukherjee[1], Shuibing Chen[1,2,‡] and Mingming Hao[1,‡]

ABSTRACT

Pancreatic islet dysfunction leading to insufficient glucose-stimulated insulin secretion triggers the clinical onset of diabetes. How islet dysfunction develops is not well understood at the cellular level, partly owing to the lack of approaches to study single islets longitudinally *in vivo*. Here, we present a noninvasive, high-resolution system to quantitatively image real-time glucose metabolism from single islets *in vivo*, currently not available with any other method. In addition, this multifunctional system simultaneously reports islet function, proliferation, vasculature and macrophage infiltration *in vivo* from the same set of images. Applying our method to a longitudinal high-fat diet study revealed changes in islet function as well as alternations in islet microenvironment. More importantly, this label-free system enabled us to image real-time glucose metabolism directly from single human islets *in vivo* for the first time, opening the door to noninvasive longitudinal *in vivo* studies of healthy and diabetic human islets.

KEY WORDS: *In vivo* imaging, Pancreatic islets, Glucose metabolism, Diabetes, Multiphoton microscopy, NAD(P)H

INTRODUCTION

Type 2 diabetes is characterized by insufficient insulin secretion from pancreatic islet β-cells to compensate for insulin resistance. Only a small portion of the people with insulin resistance progress to overt diabetes (Masharani and German, 2011), a transition that crucially depends on islet β-cell dysfunction (Kahn, 2003). In order to understand how type 2 diabetes risk factors, such as obesity, affect islet function, a technique is required that allows longitudinal studies of pancreatic islet function *in vivo*. Although blood insulin measurements can reflect islet function, this method is insensitive to small changes, and the readout can be complicated by other physiological activities. Noninvasive *in vivo* imaging of pancreatic islets has long remained a formidable challenge for diabetes research (Malaisse and Maedler, 2012; Virostko et al., 2006). Several of the high-resolution approaches that are currently available to image islets *in vivo* are highly invasive (Leibiger et al., 2012). Methods such as positron emission tomography (PET) and magnetic resonance imaging (MRI) offer great potential for imaging human pancreatic islets *in situ*, but they are limited by low resolution and sensitivity (Andralojc et al., 2012; Virostko et al., 2006). Although bioluminescence and fluorescence imaging has the highest sensitivity, its application is mainly restricted to evaluating islet mass and survival (Virostko et al., 2006).

An innovative *in vivo* imaging system has been developed previously to study islets that had been transplanted into the anterior chamber of the eye (Speier et al., 2008a,b). The transplanted islets in the eye (intraocular islets) have been used as optically accessible reporters of the endogenous islets, because they have similar structural and functional features as those in the native pancreas (Ilegems et al., 2013; Rodriguez-Diaz et al., 2012; Speier et al., 2008a). Despite several of its excellent utilities, the most essential application – the ability to repeatedly measure an islet's response to glucose stimulation in real time – has yet to be established. Fundamental to islet imaging, this functionality is where a technique makes the most significant contribution to diabetes research. Here, we fill the crucial gap with a high-resolution quantitative imaging system that enables *in vivo* longitudinal studies of glucose metabolism in single islets.

When selecting a method to measure real-time glucose response in intraocular islets, one must consider its applicability to human islet studies, which is the ultimate aim for any islet imaging system. Consequently, we rejected the introduction of fluorescent biosensors through genetic manipulation. We also ruled out perfusion with Ca^{2+} probes (Speier et al., 2008a) or viral transduction of fluorescent reporters because they can only label a small number of cells in the islet periphery. For these reasons, we turned to islet intrinsic autofluorescence. Endogenous fluorescent cofactor NAD(P)H is a major autofluorescence signal in the cell. Because $NAD(P)^+$ is nonfluorescent, imaging of NAD(P)H levels has been used to quantify the *in situ* redox state and mitochondrial function (Chance et al., 1962; Luciani et al., 2006; Mayevsky and Rogatsky, 2007). In pancreatic islets, a method has been established to use NAD(P)H to study glucose-stimulated insulin secretion (GSIS) *in vitro* (Bennett et al., 1996; Kiekens et al., 1992; Patterson et al., 2000; Piston and Knobel, 1999a; Rocheleau et al., 2004). Quantitative NAD(P)H imaging, as used in this study, directly measures glucose metabolism, and can be used to correlate autofluorescence signal with downstream glucose-stimulated events (Piston and Knobel, 1999b). Upon glucose entering the pancreatic β-cell, NADH is first generated through glycolysis and the citric acid cycle, contributing to a rise in the ATP to ADP ratio that eventually leads to Ca^{2+} influx and insulin secretion (Patterson et al., 2000). A rise in cytosolic Ca^{2+} is followed closely by increased mitochondrial Ca^{2+}, which activates several dehydrogenases that form NADH in the mitochondria (Denton, 2009; Kennedy et al., 1996). This interdependence between NAD(P)H and intracellular Ca^{2+} enables us to use the

[1]Department of Biochemistry, Weill Cornell Medical College, New York, NY 10065, USA. [2]Department of Surgery, Weill Cornell Medical College, New York, NY 10065, USA.
*Present address: Department of Physics, Southern Connecticut State University, New Haven, CT 06515, USA.

‡Authors for correspondence (mhao@med.cornell.edu; shc2034@med.cornell.edu)

M.H., 0000-0003-4677-5111

Received 11 April 2016; Accepted 27 May 2016

Journal of Cell Science (2016) 129, 2865-2875 doi:10.1242/jcs.190843

glucose-stimulated NAD(P)H response to measure pancreatic β-cell function. To image islet autofluorescence *in vivo*, we used multiphoton excitation microscopy because of its greater imaging depths and reduced overall photobleaching and photodamage (Benninger et al., 2008). It is the only available method for high-resolution autofluorescence imaging in a thick sample that preserves cellular viability and function (Piston and Knobel, 1999b).

Unlike other *in vivo* imaging platforms that study a single aspect of islet function at a time, we were able to simultaneously report changes in glucose metabolism as well as islet proliferation, fibrosis, vasculature and macrophage infiltration, from the same set of images. This was accomplished by uncovering multiple sources of tissue autofluorescence, which was acquired simultaneously when using multiphoton microscopy. Finally, we show for the first time that real-time glucose metabolism can be imaged directly in single human islets *in vivo* and demonstrate how this system can be applied to study human islet function during diabetes development. Because many tissues share universal autofluorescence properties, a similar *in vivo* imaging platform can be readily adopted to investigate a wide range of biological systems.

RESULTS

Multifunctional *in vivo* imaging of islet autofluorescence

Islets that had been engrafted readily after transplantation into the anterior chamber of the eye (Speier et al., 2008a) and islet autofluorescence were imaged through the transparent cornea, acting as a natural optical window (Fig. 1A; Fig. S1A–C, Movie 1). Fig. 1A shows a set of images taken of the same islets over five weeks. The second row contains merged autofluorescence images. Autofluorescence signals that had been collected simultaneously in different emission channels could be used to visualize distinct aspects of islet biology (Fig. 1B). Channel 1 (Ch1, blue) was dominated by second harmonic generation (SHG), with strong signals in the cornea and the islet. NAD(P)H was imaged in channel 2 (Ch2, green). Channel 4 autofluorescence (Ch4, red) came mainly from lipofuscin (Tsuchida et al., 1987) and porphyrin derivatives (Croce and Bottiroli, 2014). We carefully analyzed the signals from each emission channel and extracted four profiles that could be used to study an islet and its *in vivo* environment (Fig. 1C, highlighted in red in each inset image; Table S1). Collagen type I was detected in channel 1 (panel i), and NAD(P)H in islet cells gave rise to the signal in channel 2 (panel ii). Signals in channel 4 showed characteristics that suggested the detection of macrophages (panel iii) and vasculature (panel iv), distinguishable by the shape and distribution of the signal, as well as the relative signal strength in channel 2 and channel 3. Panel v of Fig. 1C demonstrates that the overwhelming majority of total autofluorescence signal came from islet cells. The NAD(P)H signal was the focus of this study and displayed a ring pattern around the dark nuclei (Fig. 1D, channel 2), consistent with it being mitochondrial, which accounts for most of the cellular NAD(P)H (Patterson et al., 2000). The subcellular resolution of the NAD(P)H signal in Fig. 1D was comparable to *in vitro* imaging of islet autofluorescence (Bennett et al., 1996) (Fig. S1D), indicating the possibility of using this system for *in vivo* studies of individual islet cells (see Fig. 4 later). In order to demonstrate the application of the aforementioned features using autofluorescence signals, we designed a longitudinal study (Fig. 1E) in which we fed host mice a high-fat diet (HFD), which is a widely used model for type 2 diabetes, and continuously monitored changes in islet function, collagen accumulation, macrophage infiltration, islet proliferation and vasculature growth, all from the same set of data, label free.

Continuous monitoring of islet vascularization and islet proliferation

Engrafted islets were revascularized by blood vessels from the iris (Fig. 1A, right-most column). Interestingly, the regions speculated to be blood vessels using autofluorescence were brighter in channel 4 and signal-void in channel 2 (Fig. 1B; Fig. S1C). To verify that autofluorescence can be used to study vasculature in and around engrafted islets, we first took autofluorescence images (Fig. 2A, panel i) and then re-imaged the same field after injecting dextran to label the blood vessels (Fig. 2A, panel ii). Simple image processing to select for areas positive in channel 4 and negative in channel 2 autofluorescence revealed detailed vasculature, overlapping with that labeled by dextran (Fig. 2A, panels iii and iv; Fig. S2, 3D reconstruction shown in Movie 2). Therefore, we propose autofluorescence imaging as an alternative means to investigate islet angiogenesis for longitudinal studies without repeated injection of dextran, as demonstrated in Fig. 2B–G.

Islet vascularization plays an important role in adapting pancreatic islets to metabolic changes and increase in insulin demand. Islet size and vasculature can be quantified label free over time *in vivo* (Fig. 2B,C), which is a considerable advantage over weekly dextran injections. Comparing blood vessel increase with islet size expansion in the same islet indicated that blood vessel growth preceded islet proliferation (Fig. 2D). Interestingly, although blood vessel density increased rapidly right after being fed with a HFD, it eventually returned to the same level as that at the start of HFD feeding, indicating that islet vasculature might have a propensity towards maintaining an optimum density (Fig. 2E). A similar conclusion was reached when data were pooled from all the islets tested (Fig. 2F,G). Although *in vitro* and *ex vivo* studies offer useful information on how pancreatic islet vasculature adapts to metabolic changes such as insulin resistance (Dai et al., 2013), direct visualization of weekly vasculature changes from the same islet could provide more precise characterization of the dynamic nature of the process. Because the vasculature density measured for the intraocular islets was equivalent to that found in the pancreas (Speier et al., 2008a), our platform could greatly facilitate the investigation of islet microcirculation under normal and diabetic conditions.

Continuous monitoring of macrophage infiltration

Comparing autofluorescence signals from different channels also revealed that some cells were bright in channel 4 but not in channel 2 (red circles, Fig. 3A). We hypothesized that these might be macrophages. Consistent with being mobile cells, rapid movement was detected from several of these bright cells in a time series (three circles in Fig. 3B; Fig. S3A, Movie 3), whereas some cells remained stationary (cyan box in Fig. 3B; Fig. S3A, Movie 3). Furthermore, clear cell morphology was imaged at single-cell resolution throughout the time series (Fig. S3B,C). These bright cells were most often found along blood vessels (Fig. S3D), in agreement with the location of macrophages. To confirm the identity of cells displaying strong channel 4 signal, we first took *in vitro* autofluorescence images of isolated islets and then re-imaged the same islet after immunostaining with an antibody against F4/80 (encoded by *Adgre1*), an extensively used surface marker for mouse macrophages (Leenen et al., 1994). This sequential imaging experiment showed that the high autofluorescence signal in channel 4 was generated from cells outlined with the F4/80-specific antibody (Fig. 3C, enlarged images of the areas indicated by

Journal of Cell Science (2016) 129, 2865-2875 doi:10.1242/jcs.190843

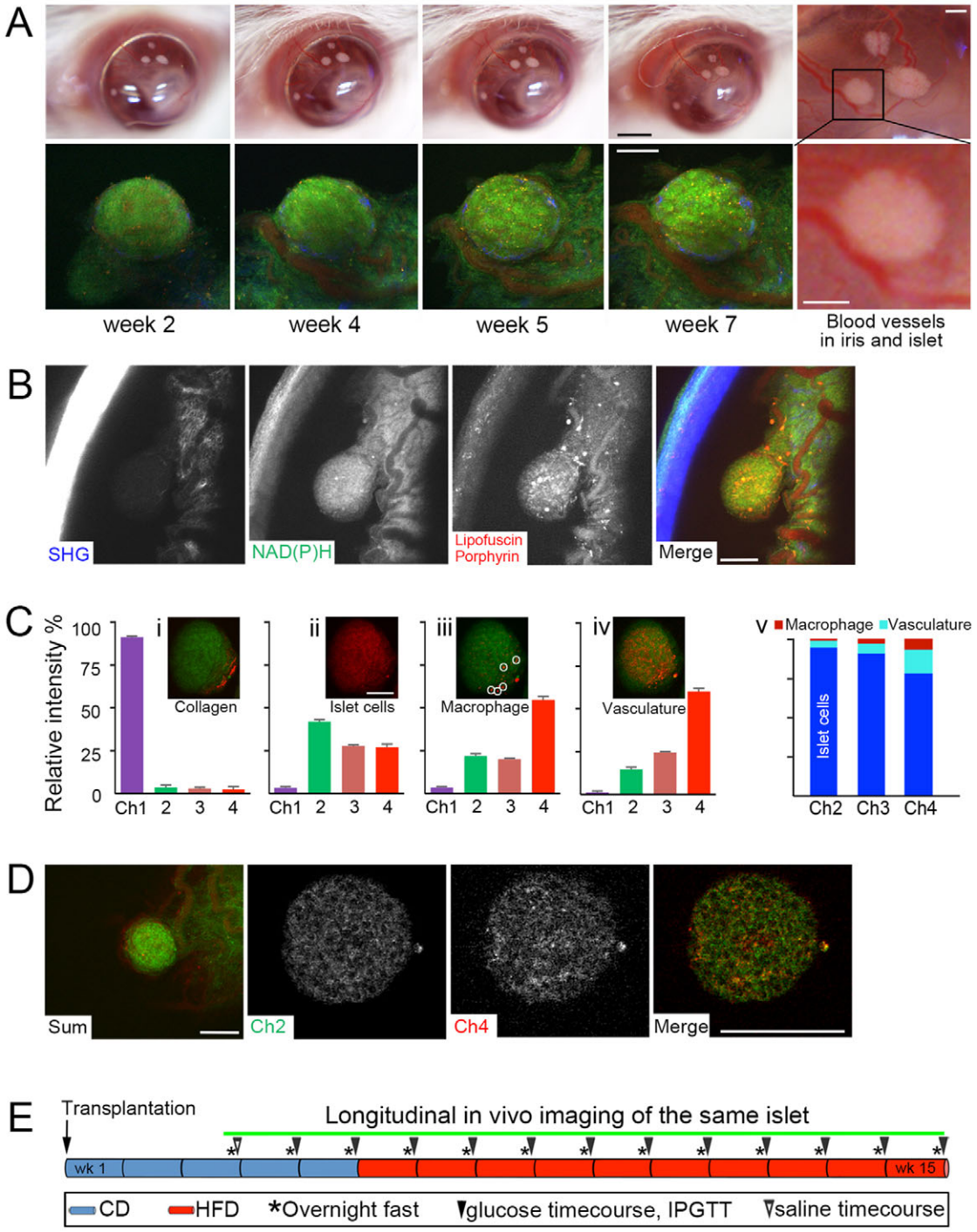

Fig. 1. Autofluorescence imaging of islets transplanted into the anterior chamber of the eye. (A) The top row shows photographs of a mouse eye containing four transplanted islets, with three enlarged on the right. The bottom row shows the merged autofluorescence images of an islet highlighted by the box. Individual channels are shown in Fig. S1C. Scale bars: 1 mm (black); 100 µm (white). (B) Sum projection images of an engrafted islet with emission from channel 1 (Ch1, blue), channel 2 (Ch2, green) and channel 4 (Ch4, red). (C) Autofluorescence spectral characteristics used to detect collagen, NAD(P)H, macrophages (circles) and vasculature. Each feature is highlighted in red. Panel v demonstrates the maximum signal contribution from macrophages and vasculature in each emission channel. (D) *In vivo* autofluorescence imaging at single-cell resolution. The first panel is a sum projection; the other panels are of single optical sections. (E) Schematic drawing of the weekly *in vivo* measurements in the longitudinal HFD study. CD, control diet. Scale bars: 100 µm (B–D).

the two white boxes), validating that the cellular structures detected in channel 4 by autofluorescence were indeed macrophages. The ability to detect macrophage accumulation in islets is important in longitudinal studies because islet inflammation has emerged as a major contributor to islet dysfunction (Eguchi and Manabe, 2013). Although macrophages could serve as scavengers for dying islet cells, as demonstrated in Fig. 7, they could also be recruited to facilitate islet cell proliferation (Brissova et al., 2014). Indeed, we often observed the autofluorescence of macrophages that were not associated with site of injury, suggesting that this label-free platform can be used to noninvasively explore the multifaceted role of macrophages in islet health and function.

Journal of Cell Science (2016) 129, 2865-2875 doi:10.1242/jcs.190843

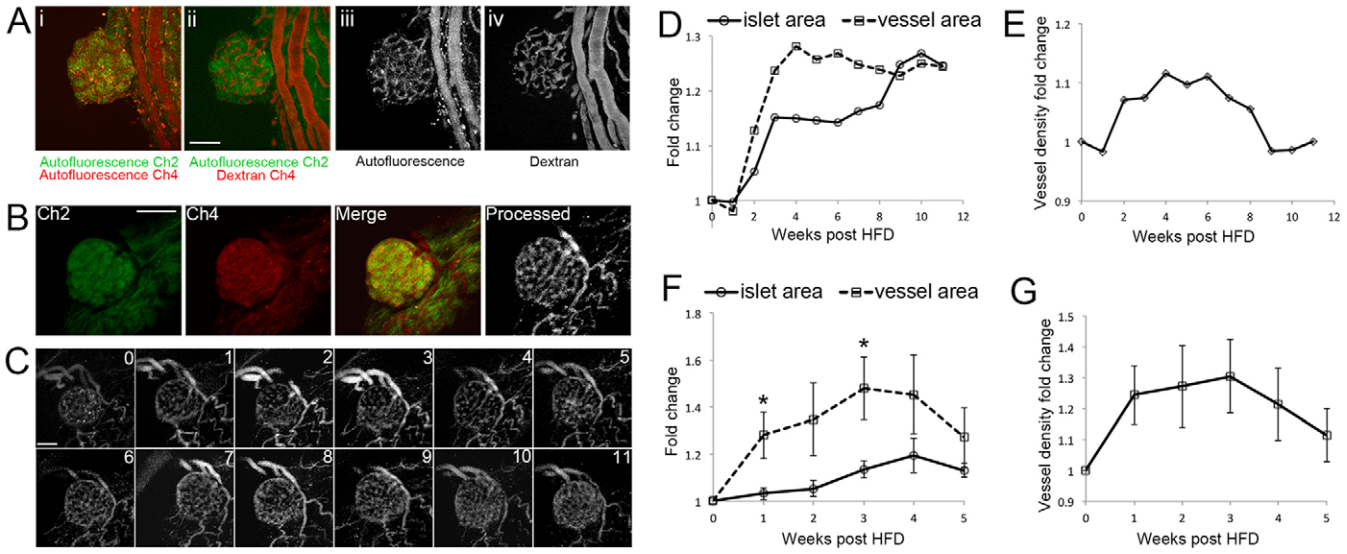

Fig. 2. Islet vascularization and proliferation in response to HFD, measured from single islets *in vivo*. (A) Islet vasculature showed a weak signal in channel 2 (green) and strong signal in channel 4 (red). Panel iii shows an autofluorescence image from channel 4, processed by excluding areas that were positive in channel 2, which can be compared with the image in panel v showing blood vessels labeled by dextran. These are maximum projection images. Single optical sections and three-dimensional images are shown in Fig. S2 and Movie 2. (B) An image of blood vessels was generated from processing the sum projection images of channel 2 (Ch2) and channel 4 (Ch4). (C) Weekly autofluorescence images of blood vessels (sum projections of ten optical sections) could be used to track islet vasculature changes. Numbers refer to the weeks on HFD. (D) Quantification of the fold change in blood vessel area (dashed line) and islet area (solid line) relative to the start of HFD feeding in the single islet presented in B. (E) Quantification of the fold change in blood vessel density, defined as blood vessel area divided by islet area, relative to that at the start of HFD, from the islet shown in B. (F) Pooled measurements of the fold change in blood vessel area (dashed line) and islet area (solid line) relative to that at the start of HFD from six islets. *P<0.05 using Student's t-test, vessel versus islet area fold increase. (G) Pooled measurement of fold change in blood vessel density relative to that at the start of the HFD in six islets from six mice. Error bars are s.e.m. Scale bars: 100 µm.

Continuous monitoring of collagen accumulation

Collagen type I is a major source of the SHG signal (Chen et al., 2012) in channel 1, which was often observed along blood vessels (Fig. 3D, arrows). Collagen accumulated in islets after feeding with a HFD (Fig. 3D,E), with the steepest increase in accumulation occurring between weeks 3 and 4. Comparison of data on the rate of fiber formation (Fig. 3E) with that of blood vessel growth (Fig. 2G) indicates that islet vasculature expansion reached its peak before collagen accumulation did in islets exposed to a HFD. We performed *in vitro* autofluorescence imaging on unprocessed pancreas tissue to verify that the fiber-like structures detected by monitoring SHG were also present in native islets (Fig. 3F). Because islet fibrosis mainly arises because of collagen type I and III accumulation, and increased fibrosis is reported in both rodent models and human subjects with diabetes (Homo-Delarche et al., 2006; Lee et al., 2011), the ability to simultaneously monitor the relative timing of vasculature growth, islet expansion, microphage infiltration and collagen accumulation is a unique tool in longitudinal studies of islet dysfunction.

Quantitative imaging of real-time *in vivo* islet response to glucose stimulation

We designed this imaging system in order to perform real-time dynamic measurements of islet response to glucose stimulation *in vivo*. To pursue this goal, we fasted the host mouse overnight to starve the intraocular islets. Three images of NAD(P)H fluorescence were taken as the basal time points. After intraperitoneal injection of glucose, a stack of ten optical sections was taken every 3 min for 45 min (Fig. 4A, sum projection images). Stack z-sections from three time points (Fig. 4B, left) and sum projection images from all time points (Fig. 4B, right) were pseudocolored to highlight the increase in NAD(P)H signal after glucose injection compared with the three basal images (t<0). When normalized to the basal signal, an average of a 40–60% increase in NAD(P)H fluorescence was detected following glucose injection (Fig. 4C,D), comparable to that measured *in vitro* (Patterson et al., 2000; Piston and Knobel, 1999a). The autofluorescence signal in Ch2 contributed by macrophages and vasculature did not increase in response to glucose (Fig. S4A).

With single-cell resolution, we were also able to show that individual cells from the same islet displayed different spatiotemporal responses to glucose simulation *in vivo* (Fig. 4E–G). In this islet, the cells in the upper right area reacted to glucose first. A wave of response moved across the islet, with the lower left area catching-up last (Fig. 4E; Fig. S4B, 'warm colors' in pseudocolored images). We next picked four cells from two regions of the islet (red boxes in Fig. 4E) to measure glucose response in single islet cells (Fig. 4F,G). Quantification shows that neighboring cells might be synchronized temporally in their glucose response, as indicated by the peak NAD(P)H fluorescence from each cell (blue boxes in Fig. 4G). This real-time quantitative measurement provides direct *in vivo* evidence for functional heterogeneity in glucose sensitivity among subpopulations of cells within the same islet and reveals that functional heterogeneity might be related to differences in the metabolic redox response to glucose. The ability to measure time-resolved glucose metabolism from individual islet cells *in vivo* is crucial to understanding intra-islet cell–cell communication and signaling.

Continuous measurement of glucose metabolism from a single islet *in vivo*

The true power of our system is the ability to monitor the same islet noninvasively over time, thus dramatically increasing the sensitivity for detecting small changes in islet function. To do this, the same field of view (e.g. same islet position and angle) had to be acquired

Journal of Cell Science (2016) 129, 2865-2875 doi:10.1242/jcs.190843

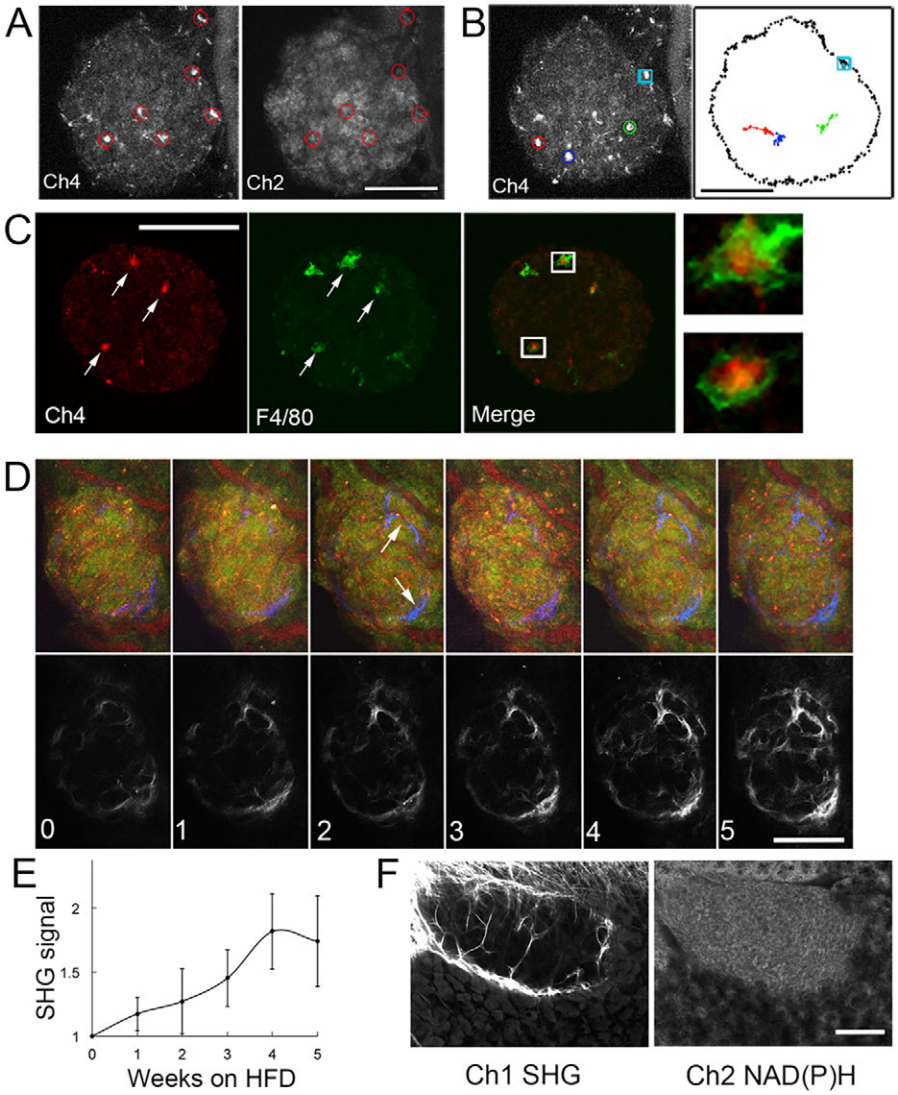

Fig. 3. Macrophage infiltration and collagen accumulation in response to HFD measured from single islets *in vivo*. (A–C) Autofluorescence detection of islet macrophages. (A) Bright signals appeared in channel 4 (Ch4) but not channel 2 (Ch2, red circles). (B) Three examples of cell movement indicated by the red, green and blue circles on the left are traced on the right. The cyan square shows a stationary cell. The complete timecourse is shown in Fig. S3 and Movie 3. (C) *In vitro* identification of the strong channel 4 autofluorescence signal as generated by macrophages as indicated by F4/80 antibody (arrows). Islets were first imaged for autofluorescence (channel 4 displayed in red) and then re-imaged after immunostaining with Alexa-Fluor-488-conjugated anti-F4/80 antibody (channel 3 is displayed in green). Contrast has been adjusted for the enlarged images. (D) Collagen accumulation detected by SHG (blue). Arrows point to fiber-like structures along blood vessels (red). Numbers refer to the weeks on the HFD. (E) Quantification of SHG signal area divided by islet area, expressed as the fold change relative to that at the start of the HFD. (F) *In vitro* autofluorescence imaging shows that a SHG signal (channel 1, Ch1) similar to that detected in intraocular islets was present in an islet in the unprocessed pancreas tissue (indicated by the channel 2 signal). Scale bars: 100 µm.

for each weekly measurement (Fig. S4C). We observed that an islet that was responsive to glucose showed a similar glucose-stimulated NAD(P)H response between measurements (Fig. 5A). By contrast, a non-responsive islet (three out of 29 islets imaged) remained non-responsive to glucose for all measurements (Fig. 5B), displaying a similar response to glucose as to saline. This consistency is key to being able to assign small and sudden functional changes to altered islet physiology instead of experimental fluctuations, as demonstrated in Figs 6 and 7. We calculated the area under curve (AUC) from the NAD(P)H signal as a convenient parameter to quantify changes in islet function over time under different conditions. Using a reference line that indicated no change relative to basal conditions (Fig. 5A,B, dotted lines), curves that fell below the reference line gave negative AUC values. Examples given in Fig. 5C are measurements from two responsive islets (black and dark gray), a non-responsive islet (light gray) and islets in response to saline injection (white). Averaged AUC values from pooled measurements are shown in Fig. 5D.

We conducted a longitudinal study to continuously monitor the function of single islets that had been exposed to a HFD for up to 24 weeks (Fig. 1E). To our knowledge, this is the first-of-its-kind *in vivo*, functional investigation of pancreatic islets based on real-time glucose metabolism. Measurements were performed once a week in order to demonstrate the temporal sensitivity of this system. At least three weekly measurements were taken under control diet conditions to establish islet function before the host mouse was switched to a HFD. A weekly 45-min time course of the glucose-stimulated NAD(P)H response was recorded for each islet, during which blood glucose was also measured at five time points on the microscope stage (intraperitoneal glucose tolerance test, IPGTT).

Fig. 6A shows sum projection images of the same islet monitored over time, and weekly glucose-stimulated NAD(P)H curves are presented in Fig. 6B. For this particular islet, the glucose response gradually increased after switching to a HFD (Fig. 6C). The average of pooled NAD(P)H AUC values under HFD conditions was significantly higher than that of the control diet (Fig. 6D). The AUC values displayed rhythmic variations (Fig. 6C), providing *in vivo* evidence that islet function might fluctuate according to physiological cues. As with any biological sample, individual islets differed widely in their response to glucose. Compared with conventional measurements that only report an averaged glucose response from a group of islets, our method of continuous *in vivo* monitoring of the same islet markedly increased the detection sensitivity, demonstrating the crucial importance of dynamic real-time measurements for detecting temporal changes in islet function.

Journal of Cell Science (2016) 129, 2865-2875 doi:10.1242/jcs.190843

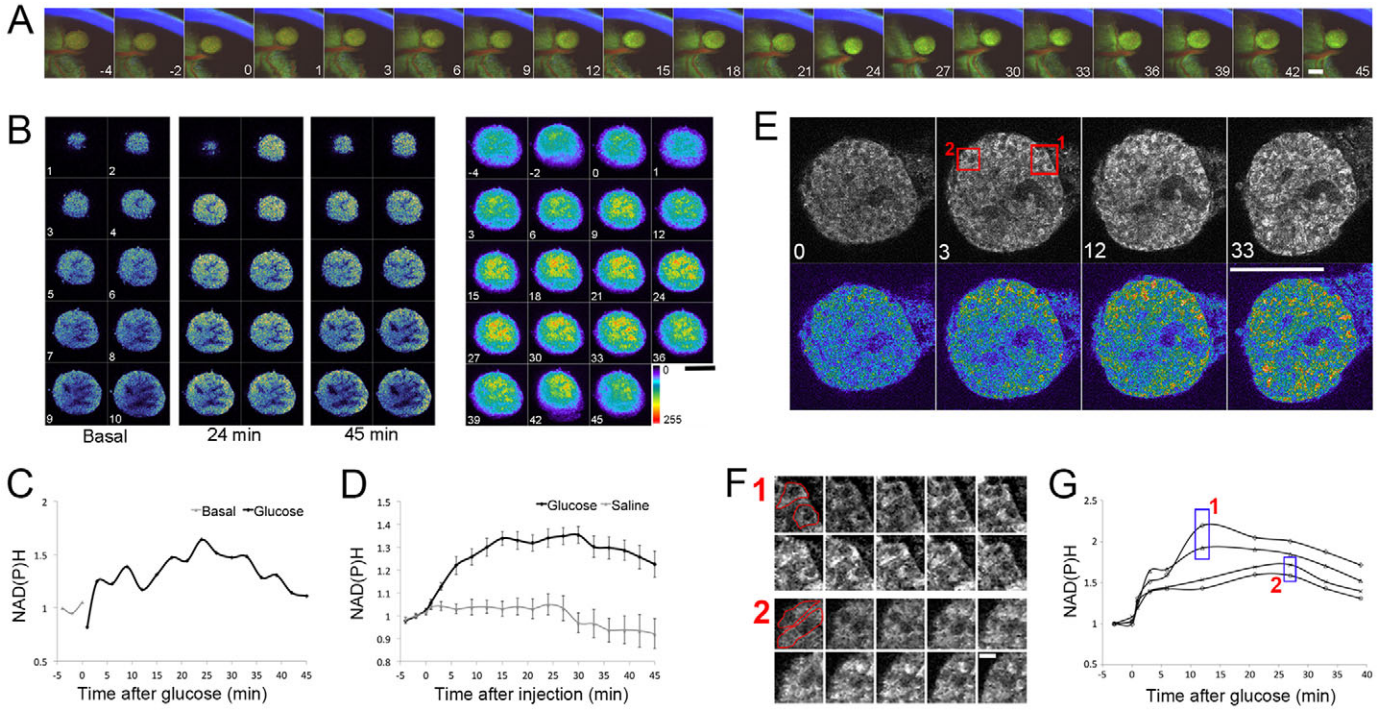

Fig. 4. Real-time *in vivo* islet NAD(P)H response to intraperitoneal injection of glucose. (A) Merged sum projection images of channel 1 (blue, cornea), channel 2 [green, NAD(P)H] and channel 4 (red, blood vessels) at each time point (min) after glucose injection. (B) Time series of the glucose-stimulated increase in NAD(P)H levels in an engrafted islet following glucose injection. Left, three representative time points, each containing a stack of ten optical sections, with the numbers labeling the position of the optical sections (top of islet to bottom of islet). Right, sum projection images from all time points, with the numbers labeling the time (min) after glucose injection. The images are pseudocolored to better show changes in islet autofluorescence. (C) Quantification of NAD(P)H autofluorescence changes from the single islet shown in B, normalized to that under basal conditions. (D) Average NAD(P)H time series in response to glucose injection (black, *n*=41 from 13 mice) and saline injection (gray, *n*=15 from 15 mice). Error bars are s.e.m. (E) Single-cell resolution detects spatiotemporal heterogeneity in islet cell response to glucose *in vivo* at time points (min) after glucose injection. The lower panels are pseudocolored to highlight the signal increase. See also Fig. S4B. (F) NAD(P)H time series of the regions outlined by the two red boxes in E, taken from the complete time series shown in Fig. S4B. (G) NAD(P)H quantification of the four cells outlined in F. The blue boxes highlight peak fluorescence levels. Scale bars: 100 µm (A,B,E); 10 µm (F).

In addition to repeatedly measuring real-time islet function *in vivo*, our system can report multiple other parameters that are crucial to islet physiology (Figs 1–3). The example shown in Fig. 7 was selected because although islet 1 behaved like the other intraocular islets, islet 2 was an anomaly owing to impurity from islet isolation, thus offering a unique opportunity to investigate islet cell death, macrophage infiltration and islet function simultaneously. At week 5 after transplantation, islet 2 was surrounded by cells that showed high fluorescence in channel 4, causing it to split abruptly (arrows) and gradually reduce in size (Fig. 7A,B). This observation was in agreement with macrophages being recruited to the islet and acting as scavengers to clear away debris. Islet 1, by contrast, expanded 196% in a two-dimensional projected area over time (Fig. 7A insets, Fig. 7C), consistent with islet proliferation in response to a HFD or obesity (Hull et al., 2005; Ilegems et al., 2013). An increase in blood vessel area correlated well with increased islet size only for islet 1 (Fig. 7C,D). Interestingly, although the number of viable cells decreased in islet 2 over time, islet function from the remaining cells, measured by glucose-stimulated NAD(P)H response per unit area, remained fairly constant over the course of the study (Fig. 7E). When islet 2 disintegrated completely in the last week of imaging, there was a

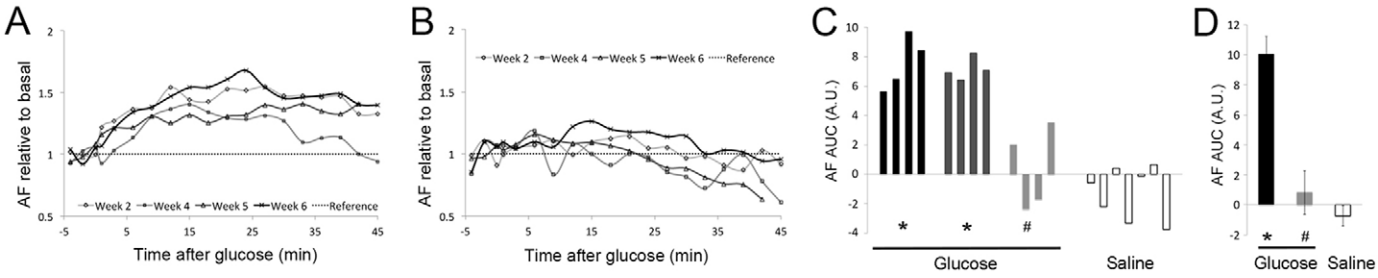

Fig. 5. Longitudinal measurements of glucose response in the same islet *in vivo*. (A,B) Examples of four weekly timecourse traces of an islet that was responsive to glucose injection (A) and one that was nonresponsive (B). (C) The AUC was quantified for the islet in A (black bars) and in B (light gray bars). AUC values from another glucose-responsive islet (dark gray bars) and the AUC response to saline (white bars) are also included. The areas below the reference line in A and B, indicating a decrease in NAD(P)H compared with basal, contribute to negative AUC values. (D) Average AUC from glucose-responsive (black, *n*=35 from 11 mice), glucose-nonresponsive (gray, *n*=10 from three mice) and saline-stimulated (white, *n*=7 from seven mice) islets. Error bars are s.e.m. **P*<0.05 and #not significant versus saline using Student's *t*-test.

Journal of Cell Science (2016) 129, 2865-2875 doi:10.1242/jcs.190843

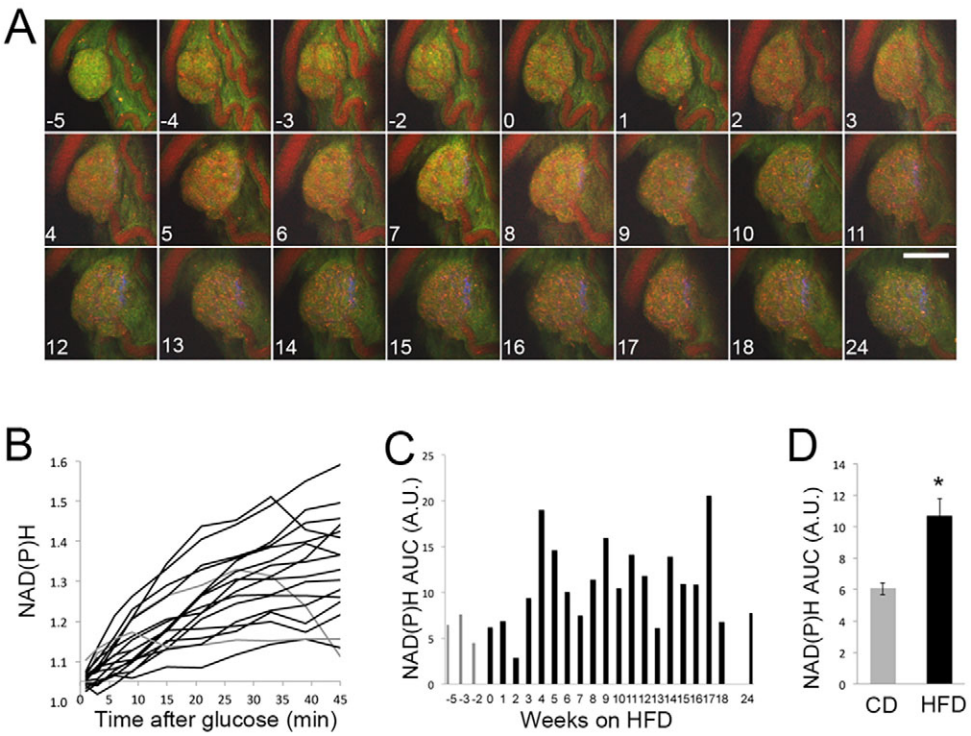

Fig. 6. Longitudinal study of real-time islet function *in vivo* using a HFD model. (A) Sum projection images of an islet during the longitudinal study. Scale bar: 100 µm. The numbers refer to weeks after the start of a HFD. (B–D) Individual weekly NAD(P)H curves (B), NAD(P)H AUC values (C) and pooled NAD(P)H AUC values generated from the data shown in C (D). The control diet (CD) data were from three weekly measurements taken while the host mouse was on a control diet before it was switched to a HFD. The gray lines (B) and bars (C,D) indicate data before starting the HFD. **P*<0.05 using Student's *t*-test. Error bars are s.e.m.

sudden termination in islet response from all remaining cells (Fig. 7E). Results from islet 2 suggest that a threshold (cliff) to islet function might exist and that an islet might lose its function all at once rather than gradually over time. The fact that we never saw a correlation between decrease in islet size and decrease in function per cell could provide *in vivo* evidence for separate regulation of islet mass and function, facilitated greatly by single islet imaging.

In vivo imaging of real-time glucose metabolism in single human pancreatic islets

It is well established that there are many important structural and functional differences between human and rodent islets (Brissova et al., 2005; Cabrera et al., 2006; Dai et al., 2012). Because our system is completely label free, it is ideally suited to studying human islets that have been transplanted in immune-deficient mice, creating humanized mouse models. Continuous imaging was performed for six months on human islets that had been transplanted into SCID-Beige mice (Fig. 8A). Autofluorescence from human islets was much higher than that from the surroundings (channel 2, Fig. 8A top row), forcing us to saturate the islet signal in order to show vasculature in the eye (Fig. 8A, bottom row). When displayed using the same dynamic range in channel 2 (green) and channel 4 (red), human islets appeared red as opposed to green for mouse islets (Fig. 8B, merge). A likely source of high channel 4 autofluorescence could be lipofuscin that had accumulated in the aging human islets. Because of the extensive colocalization between the channel 2 and channel 4 signals in human islets (correlation coefficient 0.82 vs 0.42 in mouse islets, right panels in Fig. 8B), we hypothesized that the bright dots in channel 2 might also be a signal from lipofuscin, because lipofuscin is known to have a broad spectrum (Tsuchida et al., 1987). The bright structures did not colocalize with thioflavin-S, which labels islet amyloid polypeptide (not shown). The intensity values in these structures did not increase with glucose (red line, Fig. S4D), and their contribution to the total change in signal intensity of islets was low (blue line versus green line, Fig. S4D).

Real-time glucose metabolism from single human islets was imaged *in vitro* (Fig. 8C) and for the first time *in vivo* (Fig. 8D). Although the NAD(P)H response rapidly reached a plateau *in vitro*, it peaked around 15 min and decreased afterwards *in vivo*. This observation suggests that there might be a difference between glucose metabolism measured from human islets *in vivo* and *in vitro*. We applied our imaging system to a longitudinal study, which showed a stable glucose response over a period of 155 days (Fig. 8E) and provided a glimpse of how single human islets respond to glucose *in vivo*. We also validated *in vitro* that there was a significant difference in the glucose-stimulated NAD(P)H response between islets from a healthy donor and islets from a type 2 diabetes donor (Fig. 8F), confirming that autofluorescence imaging could be used to study human islets under different disease states. The type 2 diabetes islets from the same donor also secreted less insulin in response to glucose (Fig. 8G), but their total insulin content was not reduced compared with that of the healthy islets (Fig. 8H). Our human islet data demonstrate the possibility of performing longitudinal *in vivo* functional studies on single human islets from healthy, pre-diabetic and type 2 diabetes individuals. Its applications to diabetes research will help fill a major gap in our knowledge of human islet function *in vivo*.

DISCUSSION

Longitudinal studies of islet response to glucose *in vivo* are key to understanding the mechanisms of islet dysfunction and discovering means to effectively preserve islet function in the fight against diabetes. It has long been a challenge in the β-cell field to perform noninvasive high-resolution imaging of real-time glucose metabolism *in vivo* (Andralojc et al., 2012). It is even more difficult to investigate *in vivo* islet function at the cellular level. Here, we describe a novel *in vivo* imaging platform for longitudinal studies of diabetes development. The key features of this technique include its noninvasiveness, real-time sensitivity, high spatiotemporal resolution and independence from exogenous

Journal of Cell Science (2016) 129, 2865-2875 doi:10.1242/jcs.190843

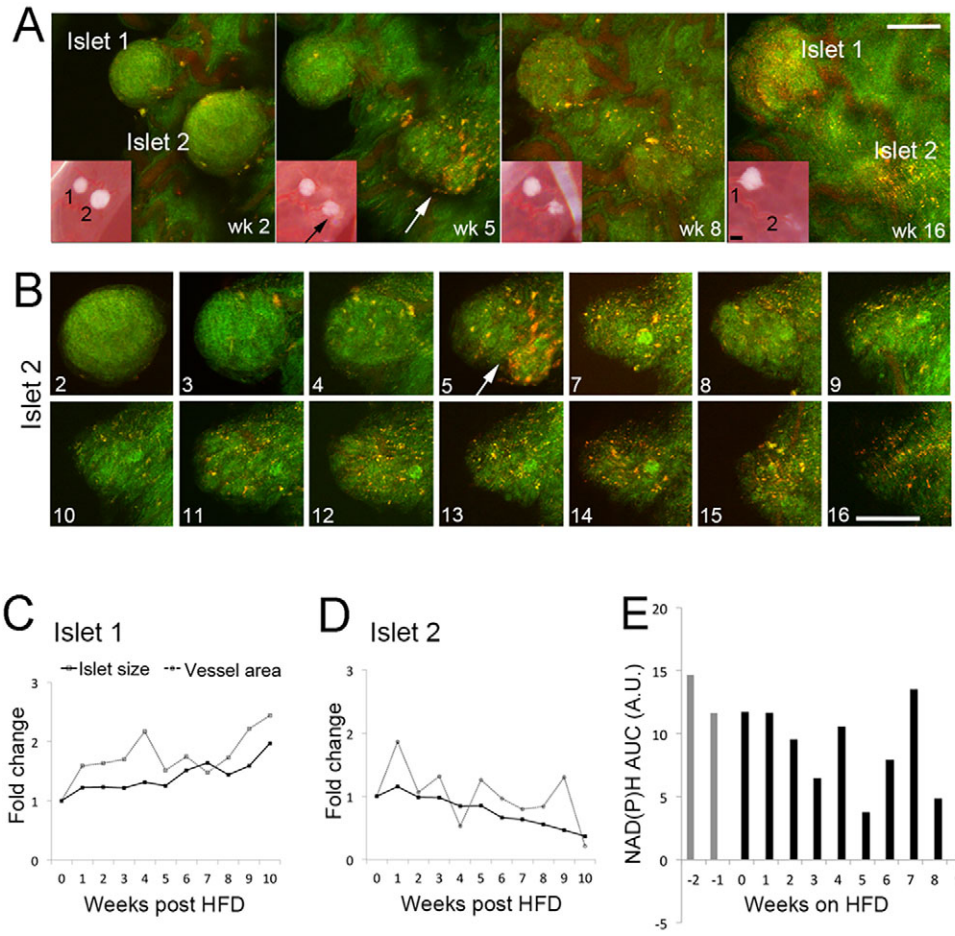

Fig. 7. Multiple islet parameters measured simultaneously in the same islet *in vivo* using a HFD model. (A,B) Accumulation of cells that were bright in channel 4 (red) leads to degradation in islet 2, consistent with the scavenging activity of macrophages. Numbers refer to the weeks after transplantation. Islet 2, surrounded by an increasing number of bright cells in channel 4, split apart at week 5 after transplantation (arrows) and gradually disintegrated over time. The insets in A show the two islets from photographs of the eye, similar to those in Fig. 1A. Scale bars: 100 µm. (C,D) Quantification of islet area (solid line) and vessel area (dotted line) over time for the two islets shown in A. (E) AUC values from glucose-stimulated NAD(P)H curves for islet 2.

labeling. A unique feature of our multifunctional imaging system is its ability to measure different parameters simultaneously from the same set of data. By examining the interactions between islet cells and vasculature, proliferation, fibrosis and macrophage infiltration under different settings, it is a powerful tool to study how key factors in diabetes development are associated with and influenced by each other. We show that it is now possible to perform functional studies on the same single islets, including human islets, for up to six months. Although the results from our longitudinal study are preliminary, they demonstrate how this imaging technique, when applied to various rodent models of diabetes, can provide unprecedented access to investigating islet dysfunction *in vivo*.

Our label-free system makes it readily transferable to *in vivo* human islet studies, thus harnessing the true power of humanized mice for disease modeling (Greiner et al., 2011). Human islet transplantation has been used to treat type 1 diabetes for decades. Current transplantation studies depend on enzyme-linked immunosorbent assay (ELISA)-based GSIS, which cannot distinguish individual islets that work well from those that do not. With our system, survival, angiogenesis, proliferation and glucose metabolism can be imaged directly from single human islets *in vivo*. This platform can be broadly used to evaluate the effectiveness of different transplanted cells and how cell niche and encapsulation materials affect human transplantation outcome.

Owing to the weekly fasting schedule required for glucose stimulation, our HFD model had only a mild effect on body weight and IPGTT, which was a limitation of our HFD study. By contrast, we might have inadvertently prolonged the time course of HFD-induced metabolic stress, thereby enabling us to better characterize the initial stage of islet pathophysiology. The weekly real-time functional imaging combined with same-islet tracking provided enhanced detection sensitivity and temporal resolution to uncover small changes in islet function. With an optimized HFD regime, we are conducting a separate longitudinal study on a large number of islets to better dissect the interrelated effects of islet dysfunction and insulin resistance in the pathogenesis of type 2 diabetes.

The imaging platform presented here is by no means limited to studying pancreatic islets. Many tissues, from human fetal brain (Epstein et al., 1992) to rat beating heart (Olson and Seiger, 1976) to human tumors (Niederkorn, 2002), have been transplanted into the anterior chamber of the eye. Autofluorescence signals are well suited to serve as intrinsic biomarkers and can provide detailed molecular information under physiologic and disease states (Richards-Kortum and Sevick-Muraca, 1996; Zipfel et al., 2003). The redox state and mitochondrial function can be monitored by quantification of cellular NAD(P)H (Mayevsky and Rogatsky, 2007; Piston and Knobel, 1999a). Spatiotemporal partitioning of glycolytic and oxidative metabolism can be resolved by measuring cytoplasmic and mitochondrial NAD(P)H changes (Patterson et al., 2000). The different roles of NADH and NAD(P)H in ATP production and antioxidant defense can be separated by simultaneously measuring two-photon NAD(P)H and one-photon lipoamide dehydrogenase autofluorescence (Rocheleau et al., 2004) or by fluorescence lifetime imaging (Blacker et al., 2014). The dynamics of lipid partitioning and fatty acid oxidation can be modeled by monitoring electron transfer flavoprotein autofluorescence (Lam et al., 2012). Finally, quantitative studies using cellular autofluorescence have revealed distinct differences

Journal of Cell Science (2016) 129, 2865-2875 doi:10.1242/jcs.190843

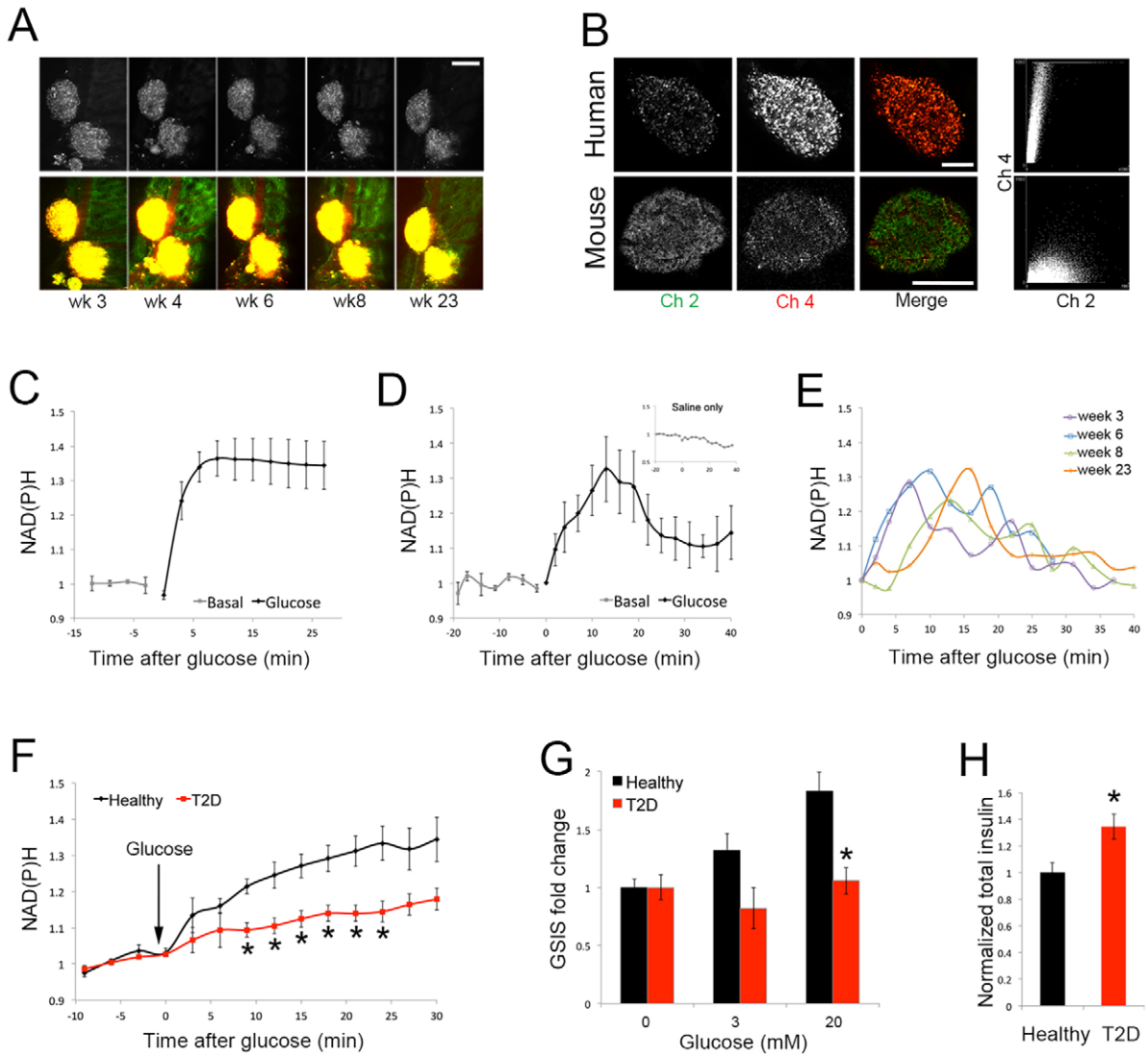

Fig. 8. Longitudinal *in vivo* imaging of single human islets. (A) Human islets that had been transplanted and engrafted into the eye of an immune-deficient SCID-Beige mouse. Top, NAD(P)H signal from channel 2; bottom, merged images of enhanced signals from channel 2 (Ch2, green) and channel 4 (Ch4, red) to show the vasculature and iris around the islets. (B) Comparison of *in vivo* autofluorescence from an engrafted human (top) and mouse (bottom) islet in the eye. The two channels (channel 2 green and channel 4 red) in each islet are displayed to the same scale. Right, pixel correlation between channel 2 (*x*-axis) and channel 4 (*y*-axis), scaled to the maximum intensity of each channel. (C) *In vitro* NAD(P)H response to glucose from isolated human islets (n=3). (D) *In vivo* NAD(P)H response to intraperitoneal glucose injection from engrafted human islets (n=8 from two mice). (E) Four weekly NAD(P)H curves in response to glucose injection from the same engrafted human islet measured *in vivo* over 23 weeks. (F) *In vitro* glucose-stimulated NAD(P)H response from healthy (black line, n=5) and type 2 diabetes (T2D, red line, n=5) islets. (G) *In vitro* GSIS from healthy (black bars) and type 2 diabetes (red bars) islets. (H) Total insulin from healthy (black bar) and type 2 diabetes (red bar) islets. Islets used in F–H were from the same healthy and type 2 diabetes donors. Each bar in G and H was derived from three samples of 20 islets each. Error bars are s.e.m. *P<0.05 between healthy and type 2 diabetes islets using Student's t-test. Scale bars: 100 µm.

between healthy and cancer cells (Butte et al., 2005; Mayevsky and Barbiro-Michaely, 2013; Pavlova et al., 2008). As multiphoton excitation microscopy, fluorescence lifetime imaging and time-resolved fluorescence anisotropy techniques become readily available from commercial sources, applying measurements of autofluorescence to intraocular imaging will enable *in vivo* longitudinal studies in a variety of biological systems.

MATERIALS AND METHODS

Animals

Both islet donors and recipients (hosts) were healthy male 8–12-week-old FVB/NJ mice (Jackson Laboratory). All animal work was approved by the Institutional Animal Care and Use Committee and Research Animal Resource Center at Weill Cornell Medical College. For the longitudinal study involving a HFD (60% fat, Research Diets, Cat# D12492), host mice were first kept on a control diet (10% fat, Research Diets, Cat# D12450J) for 5 weeks after islet transplantation before switching to a HFD.

Transplantation

Islet isolation was performed following the literature (Carter et al., 2009) with minor modifications. Collagenase P (Roche) was first perfused through the common bile duct for digestion. Islets were separated from exocrine cells by gradient centrifugation using Histopaque 1077 and 1119 (Sigma), and further purified by manual picking. Control human islets (InSphero) were cultured in SD InSight Cell-Culture medium (InSphero). Healthy and type 2 diabetes islets came from the Integrated Islet Distribution Program and were cultured in RPMI 1640 (Gibco) with 10% FBS overnight before transplantation. Islet transplantation was carried out as described previously (Speier et al., 2008b) with modifications. A 26-G needle was

used to puncture a hole in the cornea, through which a 26-G cannula was inserted, and 20–40 purified islets were injected per eye.

Longitudinal *in vivo* imaging

For imaging, the host mouse was anesthetized with fentanyl, midazolam and haloperidol, at 0.65, 12.5 and 12.5 mg per kg body weight, respectively. This cocktail of anesthetics was specifically optimized for minimum interference with *in vivo* glucose metabolism. The mouse was held in a mouse holder (Speier et al., 2008b) with a nose piece to supply oxygen. Islet autofluorescence was imaged with an Olympus FluoView FV1000MPE upright multiphoton microscope, using Spectra Physics Mai Tai Deepsee femto-second pulsed laser for excitation (755 nm) and a 25× water-immersion lens (numerical aperture 1.05) that allowed imaging up to 0.25 mm in depth. There was no long-term photodamage for *in vivo* islet imaging, as evidenced by the stable weekly redox response to glucose over 6 months. Fluorescence signals were acquired through a customized filter set with the following bandwidths: 360–400 nm for channel 1, 420–490 nm for channel 2, 500–550 nm for channel 3 and 550–650 nm for channel 4.

Each week before imaging, host mice were fasted sequentially on the day before for 20–22 h. Before autofluorescence imaging, white light photographs of the mouse eyes were taken using an Olympus DP20 camera, in order to document the location of the transplanted islets. At the beginning of each imaging session, a stack oversampling the whole islet was taken for islet size and blood vessel density measurement. To monitor autofluorescence changes in response to glucose stimulation, a stack of ten *z*-sections covering the top 45 µm of the islet was taken at each time point. Three stacks were taken before glucose administration to establish the basal signal. Intraperitoneal glucose injection was then carried out at 2 g per kg body weight using 20% glucose dissolved in saline. After glucose injection, islet stacks were taken at different time points. Blood glucose was also measured at basal and four time points after glucose administration, each immediately following autofluorescence imaging, using a drop of tail blood on a glucose meter (IPGTT). During imaging, the mice were placed on a heated microscope stage insert set at 37°C, with oxygen supplementation through a nose cone. They received warm 20% glucose in saline during recovery on a heating pad.

In vitro autofluorescence imaging of isolated islets

Islets were seeded in 6-well plastic dishes and allowed to recover overnight after isolation. Autofluorescence imaging was performed using the same acquisition settings as that used for *in vivo* imaging. To validate macrophage identification with antibody staining, a set of autofluorescence images was first acquired. The islets were then immunostained with Alexa-Fluor-488-cojugated anti-F4/80 antibody (1:100; cat no MCA497A488T) for 1 h at 37°C, and re-imaged using the same settings in order to ensure a good NAD(P)H signal to identify islet cells. Peak intensity was detected in channel 3 for Alexa-Fluor-488. To confirm the presence of an SHG signal in the native pancreas, a set of autofluorescence images was first acquired on a piece of unprocessed freshly harvested pancreas tissue. The same piece of tissue was then fixed in 10% formalin overnight, paraffin embedded, sectioned and stained with hematoxylin and eosin to identify the islet imaged by autofluorescence.

Image analysis

Image analysis was performed using MetaMorph (Molecular Devices). For display, sum projections of each channel were produced, color-coded (channel 1 blue, channel 2 green, channel 4 red) and merged, to generate the final sum image. NAD(P)H fluorescence was quantified using sum projection images of channel 2 from each time point. Islets were manually outlined to measure autofluorescence intensity per pixel. Three adjacent cell-free areas were selected to measure background intensity. To calculate fold change, background-corrected intensity at each time point was normalized to the average intensity of the three basal images. Weekly glucose-stimulated NAD(P)H curves were displayed using a moving average in the figures to emphasize key data features without the point-to-point fluctuations contributed by live-animal imaging. To generate islet vasculature images, a background-corrected channel 4 image was divided by the corresponding background-corrected channel 2 image to highlight the pixels enriched in channel 4. The resulting ratio image was then used to subtract the background-corrected channel 2 image to select for pixels that were bright in channel 4 and dim in channel 2. We manually outlined the blood vessels to measure the two-dimensional projected area. Correlation coefficients between channel 2 and channel 4 in human and mouse islets were measured as described (Bogan et al., 2012). Pseudocolor images were generated using a built-in pseudocolor lookup table in MetaMorph. To determine the spectral properties of different autofluorescence sources, three islets under basal glucose with the largest number of detectable macrophages were selected for quantification. Within each islet, three areas of each component were measured based on a single plane. Macrophages and lipofuscin were distinguished in part by size, with macrophages defined as being over 50 μm^2 and lipofuscin dots less than 10 μm^2.

Statistical analysis

Results were expressed as mean±s.e.m. A two-tailed unpaired Student's *t*-test was used to calculate *P*-values. Differences were considered statistically significant at $P<0.05$. After establishing the pre-diet islet function, host mice were paired according to their glucose-responsiveness and then divided randomly into HFD and control diet groups, where *n* denotes the number of mice used. For all the other measurements, *n* denotes the number of times the measurement was performed.

Acknowledgements

The authors are grateful to Dr Stephan Speier and Dr Rodolfo J. Ricart Arbona for technical advice. We would like to thank Dr David Piston for critical reading of the manuscript. All imaging was carried out at the Optical Microscopy Core Facility of Weill Cornell Medical College.

Competing interests

The authors declare no competing or financial interests.

Author contributions

M.H. and S.C. conceived the project. M.H. designed and G.L. established the real-time *in vivo* islet functional assay using intraocular islet autofluorescence imaging. M.H., G.L., S.M., B.W. and S.C. planned the experiments. G.L. and M.G.W. performed the islet transplantation. G.L. and B.W. performed the imaging. A.C.N.C. measured GSIS from human islets. G.L., M.H., S.M. and B.W. analyzed the data. M.H. and G.L. wrote the manuscript.

Funding

This work was supported in part by the National Center for Advancing Translational Sciences of the National Institutes of Health [grant number UL1TR000457 (to M.H.)]; New York Stem Cell Foundation [grant number R-103 (to S.C.)]; and the National Institutes of Health [grant number DP2 DK098093-01 (to S.C.)]. S.C. is New York Stem Cell Foundation-Robertson Investigator. Deposited in PMC for release after 12 months.

Supplementary information

Supplementary information available online at
http://jcs.biologists.org/lookup/doi/10.1242/jcs.190843.supplemental

References

Andralojc, K., Srinivas, M., Brom, M., Joosten, L., de Vries, I. J. M., Eizirik, D. L., Boerman, O. C., Meda, P. and Gotthardt, M. (2012). Obstacles on the way to the clinical visualisation of beta cells: looking for the Aeneas of molecular imaging to navigate between Scylla and Charybdis. *Diabetologia* **55**, 1247-1257.

Bennett, B. D., Jetton, T. L., Ying, G., Magnuson, M. A. and Piston, D. W. (1996). Quantitative subcellular imaging of glucose metabolism within intact pancreatic islets. *J. Biol. Chem.* **271**, 3647-3651.

Benninger, R. K. P., Hao, M. and Piston, D. W. (2008). Multi-photon excitation imaging of dynamic processes in living cells and tissues. *Rev. Physiol. Biochem. Pharmacol.* **160**, 71-92.

Blacker, T. S., Mann, Z. F., Gale, J. E., Ziegler, M., Bain, A. J., Szabadkai, G. and Duchen, M. R. (2014). Separating NADH and NADPH fluorescence in live cells and tissues using FLIM. *Nat. Commun.* **5**, 3936.

Bogan, J. S., Xu, Y. and Hao, M. (2012). Cholesterol accumulation increases insulin granule size and impairs membrane trafficking. *Traffic* **13**, 1466-1480.

Brissova, M., Fowler, M. J., Nicholson, W. E., Chu, A., Hirshberg, B., Harlan, D. M. and Powers, A. C. (2005). Assessment of human pancreatic islet architecture and composition by laser scanning confocal microscopy. *J. Histochem. Cytochem.* **53**, 1087-1097.

Brissova, M., Aamodt, K., Brahmachary, P., Prasad, N., Hong, J.-Y., Dai, C., Mellati, M., Shostak, A., Poffenberger, G., Aramandla, R. et al. (2014). Islet microenvironment, modulated by vascular endothelial growth factor-A signaling, promotes beta cell regeneration. *Cell Metab.* **19**, 498-511.

Butte, P. V., Pikul, B. K., Hever, A., Yong, W. H., Black, K. L. and Marcu, L. (2005). Diagnosis of meningioma by time-resolved fluorescence spectroscopy. *J. Biomed. Opt.* **10**, 064026.
Cabrera, O., Berman, D. M., Kenyon, N. S., Ricordi, C., Berggren, P.-O. and Caicedo, A. (2006). The unique cytoarchitecture of human pancreatic islets has implications for islet cell function. *Proc. Natl. Acad. Sci. USA* **103**, 2334-2339.
Carter, J. D., Dula, S. B., Corbin, K. L., Wu, R. and Nunemaker, C. S. (2009). A practical guide to rodent islet isolation and assessment. *Biol. Proced. Online* **11**, 3-31.
Chance, B., Cohen, P., Jobsis, F. and Schoener, B. (1962). Intracellular oxidation-reduction states in vivo: the microfluorometry of pyridine nucleotide gives a continuous measurement of the oxidation state. *Science* **137**, 499-508.
Chen, X., Nadiarynkh, O., Plotnikov, S. and Campagnola, P. J. (2012). Second harmonic generation microscopy for quantitative analysis of collagen fibrillar structure. *Nat. Protoc.* **7**, 654-669.
Croce, A. C. and Bottiroli, G. (2014). Autofluorescence spectroscopy and imaging: a tool for biomedical research and diagnosis. *Eur. J. Histochem.* **58**, 2461.
Dai, C., Brissova, M., Hang, Y., Thompson, C., Poffenberger, G., Shostak, A., Chen, Z., Stein, R. and Powers, A. C. (2012). Islet-enriched gene expression and glucose-induced insulin secretion in human and mouse islets. *Diabetologia* **55**, 707-718.
Dai, C., Brissova, M., Reinert, R. B., Nyman, L., Liu, E. H., Thompson, C., Shostak, A., Shiota, M., Takahashi, T. and Powers, A. C. (2013). Pancreatic islet vasculature adapts to insulin resistance through dilation and not angiogenesis. *Diabetes* **62**, 4144-4153.
Denton, R. M. (2009). Regulation of mitochondrial dehydrogenases by calcium ions. *Biochim. Biophys. Acta* **1787**, 1309-1316.
Eguchi, K. and Manabe, I. (2013). Macrophages and islet inflammation in type 2 diabetes. *Diabetes Obes. Metab.* **15** Suppl. 3, 152-158.
Epstein, L. G., Cvetkovich, T. A., Lazar, E., Dehlinger, K., Dzenko, K., del Cerro, C. and del Cerro, M. (1992). Successful xenografts of second trimester human fetal brain and retinal tissue in the anterior chamber of the eye of adult immunosuppressed rats. *J. Neural Transplant. Plast.* **3**, 151-158.
Greiner, D. L., Brehm, M. A., Hosur, V., Harlan, D. M., Powers, A. C. and Shultz, L. D. (2011). Humanized mice for the study of type 1 and type 2 diabetes. *Ann. N. Y. Acad. Sci.* **1245**, 55-58.
Homo-Delarche, F., Calderari, S., Irminger, J.-C., Gangnerau, M.-N., Coulaud, J., Rickenbach, K., Dolz, M., Halban, P., Portha, B. and Serradas, P. (2006). Islet inflammation and fibrosis in a spontaneous model of type 2 diabetes, the GK rat. *Diabetes* **55**, 1625-1633.
Hull, R. L., Kodama, K., Utzschneider, K. M., Carr, D. B., Prigeon, R. L. and Kahn, S. E. (2005). Dietary-fat-induced obesity in mice results in beta cell hyperplasia but not increased insulin release: evidence for specificity of impaired beta cell adaptation. *Diabetologia* **48**, 1350-1358.
Ilegems, E., Dicker, A., Speier, S., Sharma, A., Bahow, A., Edlund, P. K., Leibiger, I. B. and Berggren, P.-O. (2013). Reporter islets in the eye reveal the plasticity of the endocrine pancreas. *Proc. Natl. Acad. Sci. USA* **110**, 20581-20586.
Kahn, S. E. (2003). The relative contributions of insulin resistance and beta-cell dysfunction to the pathophysiology of Type 2 diabetes. *Diabetologia* **46**, 3-19.
Kennedy, E. D., Rizzuto, R., Theler, J. M., Pralong, W. F., Bastianutto, C., Pozzan, T. and Wollheim, C. B. (1996). Glucose-stimulated insulin secretion correlates with changes in mitochondrial and cytosolic Ca2+ in aequorin-expressing INS-1 cells. *J. Clin. Invest.* **98**, 2524-2538.
Kiekens, R., In't Veld, P., Mahler, T., Schuit, F., Van De Winkel, M. and Pipeleers, D. (1992). Differences in glucose recognition by individual rat pancreatic B cells are associated with intercellular differences in glucose-induced biosynthetic activity. *J. Clin. Invest.* **89**, 117-125.
Lam, A. K., Silva, P. N., Altamentova, S. M. and Rocheleau, J. V. (2012). Quantitative imaging of electron transfer flavoprotein autofluorescence reveals the dynamics of lipid partitioning in living pancreatic islets. *Integr. Biol.* **4**, 838-846.
Lee, E., Ryu, G. R., Ko, S.-H., Ahn, Y.-B., Yoon, K.-H., Ha, H. and Song, K.-H. (2011). Antioxidant treatment may protect pancreatic beta cells through the attenuation of islet fibrosis in an animal model of type 2 diabetes. *Biochem. Biophys. Res. Commun.* **414**, 397-402.
Leenen, P. J. M., de Bruijn, M. F. T. R., Voerman, J. S. A., Campbell, P. A. and van Ewijk, W. (1994). Markers of mouse macrophage development detected by monoclonal antibodies. *J. Immunol. Methods* **174**, 5-19.
Leibiger, I. B., Caicedo, A. and Berggren, P.-O. (2012). Non-invasive in vivo imaging of pancreatic beta-cell function and survival - a perspective. *Acta Physiol.* **204**, 178-185.
Luciani, D. S., Misler, S. and Polonsky, K. S. (2006). Ca2+ controls slow NAD(P)H oscillations in glucose-stimulated mouse pancreatic islets. *J. Physiol.* **572**, 379-392.
Malaisse, W. J. and Maedler, K. (2012). Imaging of the beta-cells of the islets of Langerhans. *Diabetes Res. Clin. Pract.* **98**, 11-18.
Masharani, U. and German, M. S. (2011). Pancreatic hormones and diabetes mellitus. In *Greenspan's Basic & Clinical Endocrinology*, 9th edn. (ed. D. G. Gardner and D. Shoback). pp. 573-655. New York, McGraw-Hill Companies, Inc.
Mayevsky, A. and Barbiro-Michaely, E. (2013). Shedding light on mitochondrial function by real time monitoring of NADH fluorescence: II: human studies. *J. Clin. Monit. Comput.* **27**, 125-145.
Mayevsky, A. and Rogatsky, G. G. (2007). Mitochondrial function in vivo evaluated by NADH fluorescence: from animal models to human studies. *Am. J. Physiol. Cell Physiol.* **292**, C615-C640.
Niederkorn, J. Y. (2002). Immune privilege in the anterior chamber of the eye. *Crit. Rev. Immunol.* **22**, 13-46.
Olson, L. and Seiger, A. (1976). Beating intraocular hearts: light-controlled rate by autonomic innervation from host iris. *J. Neurobiol.* **7**, 193-203.
Patterson, G. H., Knobel, S. M., Arkhammar, P., Thastrup, O. and Piston, D. W. (2000). Separation of the glucose-stimulated cytoplasmic and mitochondrial NAD(P)H responses in pancreatic islet beta cells. *Proc. Natl. Acad. Sci. USA* **97**, 5203-5207.
Pavlova, I., Williams, M., El-Naggar, A., Richards-Kortum, R. and Gillenwater, A. (2008). Understanding the biological basis of autofluorescence imaging for oral cancer detection: high-resolution fluorescence microscopy in viable tissue. *Clin. Cancer. Res.* **14**, 2396-2404.
Piston, D. W. and Knobel, S. M. (1999a). Quantitative imaging of metabolism by two-photon excitation microscopy. *Methods Enzymol.* **307**, 351-368.
Piston, D. W. and Knobel, S. M. (1999b). Real-time analysis of glucose metabolism by microscopy. *Trends Endocrinol. Metab.* **10**, 413-417.
Richards-Kortum, R. and Sevick-Muraca, E. (1996). Quantitative optical spectroscopy for tissue diagnosis. *Annu. Rev. Phys. Chem.* **47**, 555-606.
Rocheleau, J. V., Head, W. S. and Piston, D. W. (2004). Quantitative NAD(P)H/flavoprotein autofluorescence imaging reveals metabolic mechanisms of pancreatic islet pyruvate response. *J. Biol. Chem.* **279**, 31780-31787.
Rodriguez-Diaz, R., Speier, S., Molano, R. D., Formoso, A., Gans, I., Abdulreda, M. H., Cabrera, O., Molina, J., Fachado, A., Ricordi, C. et al. (2012). Noninvasive in vivo model demonstrating the effects of autonomic innervation on pancreatic islet function. *Proc. Natl. Acad. Sci. USA* **109**, 21456-21461.
Speier, S., Nyqvist, D., Cabrera, O., Yu, J., Molano, R. D., Pileggi, A., Moede, T., Köhler, M., Wilbertz, J., Leibiger, B. et al. (2008a). Noninvasive in vivo imaging of pancreatic islet cell biology. *Nat. Med.* **14**, 574-578.
Speier, S., Nyqvist, D., Köhler, M., Caicedo, A., Leibiger, I. B. and Berggren, P.-O. (2008b). Noninvasive high-resolution in vivo imaging of cell biology in the anterior chamber of the mouse eye. *Nat. Protoc.* **3**, 1278-1286.
Tsuchida, M., Miura, T. and Aibara, K. (1987). Lipofuscin and lipofuscin-like substances. *Chem. Phys. Lipids* **44**, 297-325.
Virostko, J., Jansen, E. D. and Powers, A. C. (2006). Current status of imaging pancreatic islets. *Curr. Diab. Rep.* **6**, 328-332.
Zipfel, W. R., Williams, R. M., Christie, R., Nikitin, A. Y., Hyman, B. T. and Webb, W. W. (2003). Live tissue intrinsic emission microscopy using multiphoton-excited native fluorescence and second harmonic generation. *Proc. Natl. Acad. Sci. USA* **100**, 7075-7080.